Pergamon

Geochimica et Cosmochimica Acta, Vol. 67, No. 20, pp. 3925–3936, 2003

0016-7037/03 $30.00 + .00

doi:10.1016/S0016-7037(00)00262-X

Fractionation of major elements between coexisting H_2O-saturated silicate melt and silicate-saturated aqueous fluids in aluminosilicate systems at 1–2 GPa

BJORN O. MYSEN[1,*] and JESSICA SHANG[2]

[1]Geophysical Laboratory, Carnegie Institution of Washington, 5251 Broad Branch Road NW, Washington, DC 20015, USA
[2]Montgomery Blair High School, Silver Spring, MD 20910, USA

(*Received November* 5, 2002; revised 16 April 2003; *accepted in revised form April* 16, 2003)

Abstract—From experimental data in the systems Na_2O-Al_2O_3-SiO_2-H_2O, K_2O-Al_2O_3-SiO_2-H_2O at 1100°C, and CaO-Al_2O_3-SiO_2-H_2O at 1200°C in the 1–2 GPa pressure range, the solution behavior of the individual oxides in coexisting H_2O-saturated silicate melts and silicate-saturated aqueous fluids appears to be incongruent. Recalculated on an anhydrous basis, in the CaO-Al_2O_3-SiO_2-H_2O system, $CaO^{fluid}/CaO^{melt} < 1$, whereas in the Na_2O-Al_2O_3-SiO_2-H_2O and K_2O-Al_2O_3-SiO_2-H_2O systems, K_2O^{fluid}/K_2O^{melt} and $Na_2O^{fluid}/Na_2O^{melt}$ both are greater than 1. The aqueous fluids are depleted in alumina relative to silicate melt.

In the Na_2O-Al_2O_3-SiO_2-H_2O, K_2O-Al_2O_3-SiO_2-H_2O, and CaO-Al_2O_3-SiO_2-H_2O systems, fluid/melt partition coefficients for the individual oxides range between ~0.005 and 0.35 depending on oxide, bulk composition and pressure. The alkali partition coefficients are about an order of magnitude higher than that of CaO. Alumina and silica partition coefficient values in the CaO-Al_2O_3-SiO_2-H_2O system are 10–20% of the values for the same oxides in the Na_2O-Al_2O_3-SiO_2-H_2O and K_2O-Al_2O_3-SiO_2-H_2O systems.

Positive correlations among individual partition coefficients and oxide concentrations in the aqueous fluids are consistent with complexing in the fluid that involves silicate polymers associated with alkalis and alkaline earths and aluminosilicate complexes where alkalis and alkaline earths may serve to charge-balance Al^{3+}, which is, perhaps, in tetrahedral coordination. Alkali aluminosilicate complexes in aqueous fluid appear more stable than Ca-aluminosilicate complexes. *Copyright © 2003 Elsevier Ltd*

1. INTRODUCTION

Evidence for fluid-mediated transport in aqueous fluids in the crust and the upper mantle is extensive. Mineral parageneses in deep crustal rocks commonly include hydrous phases such as mica, epidote, and amphibole group minerals (e.g., Ernst et al., 1998). Their dehydration can provide a source of aqueous fluids. Experimental data delineating the stability field of hydrous minerals have been used to deduce activity of H_2O under deep crustal high-pressure metamorphism (e.g., Schreyer, 1995; Liu et al., 1996; Poli and Schmidt, 1998). Dehydration of hydrous minerals during metamorphism also has been ascribed to alteration of major and trace element contents in high-grade metamorphic rocks (e.g., Rollinson and Windley, 1980; Fowler, 1984; Whitehouse, 1989). That suggestion is supported by experimental data on trace element partitioning between fluid and relevant silicate minerals (e.g., Brenan et al., 1995, 1998; Foley et al., 1996).

In the upper mantle, aqueous fluids are particularly important near convergent plate boundaries where there is abundant evidence for fluid transport. For example, hydrous minerals such as phlogopite and amphibole in mantle-derived xenoliths imply the presence of an aqueous fluid (e.g., Aoki, 1987; Swanson et al., 1987; Ionov and Hofmann, 1995). These observations are consistent with extensive upper mantle pressure/temperature stability fields of pargasite, phlogopite, and K-richterite (Mysen and Boettcher, 1975; Sudo and Tatsumi, 1990; Konzett and Ulmer, 1999). Other evidence includes orthopyroxene overgrowth on olivine in mantle-derived ultramafic xenoliths (e.g., McInnes, 1996; Riter and Smith, 1996), which is consistent with laboratory studies of ingress of silicate-saturated aqueous fluids into peridotite mineral assemblages (Iizuka and Nakamura, 1995; Iizuka and Mysen, 1998) and with silicate solubility data for aqueous fluids in the system MgO-SiO_2-H_2O (Nakamura and Kushiro, 1974; Stalder et al., 2001; Mibe et al., 2002). Aqueous fluid-mediated alteration of trace element and isotopic abundance of source regions of magmatic liquids in island arcs by slab-derived aqueous fluids is also frequently suggested (e.g., Morris et al., 1990; Plank and Langmuir, 1993; Bebout et al., 1993; Brenan et al., 1995, 1998; Turner and Foden, 2001).

Despite the abundant evidence for water/rock interaction in crustal and mantle rocks, experimental data needed to describe the alteration processes are rare. Quantitative characterization of these processes requires knowledge of silicate solubility and solution mechanisms of silicate in H_2O-rich fluids under deep crustal and upper mantle pressure and temperature conditions. In this pressure- and temperature-range, some data are available for the system MgO-SiO_2-H_2O (Nakamura and Kushiro, 1974; Stalder et al., 2001; Mibe et al., 2002) and for the systems K_2O-Al_2O_3-SiO_2-H_2O and Na_2O-Al_2O_3-SiO_2-H_2O (Stalder et al., 2000; Mysen and Armstrong, 2002). Alkaline earth oxides such as CaO are, however, among the major components in igneous and metamorphic rocks that may undergo fluid-mediated alteration. Relevant experimental data for alkaline earth aluminosilicate systems are nearly non-existent. In this report, we will, therefore, focus on the solubility and solubility behavior of CaO, Al_2O_3, and SiO_2 in silicate-saturated aqueous solutions and compare those data with existing data on the solubility behavior of alkalis, Al_2O_3, and SiO_2 for equivalent

* Author to whom correspondence should be addressed (mysen@gl.ciw.edu).

Table 1. Composition of starting materials (wt%).[a]

	CS4	CS4A3	CS4A6
SiO_2	78.66 ± 0.49[b]	75.61 ± 1.04	75.02 ± 0.66
Al_2O_3	0.53 ± 0.24[c]	4.68 ± 0.13	9.36 ± 0.14
CaO	20.81 ± 0.16	19.71 ± 0.23	16.62 ± 0.18

[a] Glasses were prepared for electron microprobe analysis by mixing the materials with ~80% $LiBO_2$ and ~20% silicate before melting this mixture at ~1000°C. The reported analyses are recalculated to 100% by taking into account the proportion of $LiBO_2$ added.

[b] The uncertainties are those after recalculation to 100% on a $LiBO_2$-free basis. In other words, the reported uncertainties are ~4 times greater than the standard error ($\pm 1\sigma$) of the average of 10 analysis spots from the original silicate + $LiBO_2$ glass.

[c] The reported 0.53 wt% Al_2O_3 reflects 0.11 wt% Al_2O_3 in the analyses of the $LiBO_2$-diluted CS4 glass. The 0.53 wt% value is this value after recalculation on a $LiBO_2$-free basis.

compositions in the systems K_2O-Al_2O_3-SiO_2-H_2O and Na_2O-Al_2O_3-SiO_2-H_2O.

1. EXPERIMENTAL METHODS

Starting compositions in the system CaO-Al_2O_3-SiO_2-H_2O were the Al-free end-member Ca-tetrasilicate (denoted CS4) and CS4 with 3 and 6 mol% Al_2O_3 added (denoted CS4A3 and CS4A6) (see Table 1 for analyzed composition of starting materials 1).[1]

These compositions were chosen so that on a molar basis, they have Al_2O_3 and SiO_2 concentrations similar to compositions KS4, KS4A3, KS4A6, NS4, NS4A3, and NS4A6 employed to study element distribution between aqueous fluids and silicate melts in the systems K_2O-Al_2O_3-SiO_2-H_2O and Na_2O-Al_2O_3-SiO_2-H_2O by Mysen and Armstrong (2002). Instead of alkalis, an equivalent proportion of Ca was used (1Ca = 2Na = 2K). In this manner, we may compare directly the effect of metal cation type on the silicate solubility in aqueous fluid and the fractionation of alkalis, Ca, Al, and Si between silicate melt and aqueous fluid.

Anhydrous starting materials were made from mixtures of spectroscopically pure $CaCO_3$, Al_2O_3, and SiO_2 ground under alcohol for ~1 h, decarbonated during slow heating (~1.5°C/min), heated at 1650°C at 0.1 MPa for 60 min, and then quenched. After this process, starting materials CS4 and CS4A3 consist of a mixture of a silica polymorph and glass, whereas CS4A6 was a glass. The starting materials were crushed to ≥ 20 μm grain size and stored at 110°C when not in use. To make these materials amenable to electron microprobe analyses to determine their chemical composition, a portion of each starting composition was mixed with $LiBO_2$ with $LiBO_2$:silicate = 4:1, melted at 1000°C, and quenched to glass. Electron microprobe analyses, obtained with a JEOL model 8900 with 15 kV accelerating voltage and 10 nAmp beam current, recalculated to 100% silicate, are shown in Table 1.

High-pressure experiments were conducted in the solid-media, high-pressure apparatus (Boyd and England, 1960) with 3/4″-diameter, tapered furnace assemblies (Kushiro, 1976). Pressure was calibrated with the calcite-aragonite and quartz-coesite transitions and the melting point of NaCl (see Bohlen, 1984). Precision is <0.05 GPa and accuracy ≤0.1 GPa. Temperature was measured with Pt-$Pt_{90}Rh_{10}$ thermocouples with no pressure correction on the emf of the thermocouples. Temperature precision is ±1°C. Temperature accuracy is ≤10°C because the effect of pressure on the emf of the thermocouples was not calibrated (Getting and Kennedy, 1970; Mao et al., 1971).

The high-pressure experiments were conducted with a double-capsule technique slightly modified after Schneider and Eggler (1986). The anhydrous starting material (10–40 mg glass sample) was loaded into a 3 mm-OD (2.6 mm-ID) and 5–6 mm long Pt capsules perforated with 200 μm holes (~50 randomly distributed holes) and sealed by welding on both ends (Schneider and Eggler, 1986, used an inner capsule just crimped, but not sealed, on both ends). This capsule was loaded into an outer, 5-mm OD and ~10 mm long Pt capsule together with the desired amount of H_2O and welded shut (1–50 μL double-distilled and deionized H_2O was loaded with a microsyringe). Weighing errors introduced with this method were ≤1% (±0.02 mg silicate and ±0.05 mg H_2O).

The holes in the inner Pt capsule served as pathways for the aqueous fluid initially in the outer capsule to communicate with the silicate melt in the inner capsule (experiments at 1200°C were above the temperatures of the H_2O-saturated liquidus for the compositions used). In this design, the inner capsule collapsed on the sample at high pressure so that the amount of excess fluid over that dissolved in the melt in the inner capsule was essentially zero. Therefore, after temperature-quenching of an experiment, H_2O-saturated silicate melt in the inner capsule and quenched fluid (with abundant quench precipitates) in the outer capsule were physically separated. After an experiment, the inner capsule was removed and physically cleaned before opening under a 50× magnification binocular microscope. The H_2O-saturated glass in the inner capsule was then removed.

The silicate glass was dehydrated at ~1200°C for 1 h at ambient pressure. This dehydrated glass was analyzed with a JEOL 8900 electron microprobe operating at 15 kV and 10 nAmp current with a 10 × 10 μm rastered square and 30 s integration time. Before subjected to analysis, however, the anhydrous silicate glass was diluted with $LiBO_2$ ($LiBO_2$:silicate = 4:1) and remelted at 1000°C for 1 h at ambient pressure. This dilution with $LiBO_2$ was necessary because the composition of most of the silicate melts after an experiment were within the field of liquid immiscibility in the CaO-Al_2O_3-SiO_2 system at 0.1 MPa pressure (Osborn and Muan, 1960). In contrast, the $LiBO_2$-diluted samples formed a homogeneous glass on which spot analyses with the electron microprobe could be used to obtain the composition of the bulk glass.

Because of extensive precipitation of silicate from the silicate-saturated fluid during quenching, fluid extracted from the outer capsule does not represent the equilibrium composition (see Mysen, 2002a, for detailed documentation). The composition of silicate-saturated aqueous fluid in equilibrium with H_2O-saturated silicate melt at high pressure and temperature was calculated, therefore, by mass-balance using the analyzed starting glass composition and the analyzed composition of the

[1] Compositions CS4, CS4A3, and CS4A6 nominally are $CaSi_4O_9$, $[CaSi_4O_9]_{97}[Ca(Ca_{0.5}Al)_4O_9]_3$, and $[CaSi_4O_9]_{94}[Ca(Ca_{0.5}Al)_4O_9]_6$, respectively.

Table 2A. Experimental results: Melt compositions (wt%).[a]

Composition	Pressure (GPa)	Time (min)	$X_{H2}O$	X_f	SiO_2	Al_2O_3	CaO	H_2O	$LiBO_2$
CS4	1	1185	0.306 (2)	0.290 (2)	71.24 ± 0.48	—	20.55 ± 0.27	7.50 ± 0.40	80
CS4	1	1230	0.404 (2)	0.386 (2)	69.59 ± 0.45	—	22.36 ± 0.18	7.50 ± 0.40	80.06
CS4	1	1215	0.497 (1)	0.478 (2)	66.94 ± 1.81	—	24.41 ± 0.26	7.50 ± 0.40	80.05
CS4	1.3	1410	0.304 (2)	0.284 (2)	68.82 ± 0.59	—	19.21 ± 0.17	11.00 ± 0.20	80.03
CS4	1.3	1200	0.405 (3)	0.382 (3)	66.80 ± 0.58	—	21.69 ± 0.21	11.00 ± 0.20	80.03
CS4	1.3	3060	0.506 (1)	0.481 (1)	66.72 ± 0.72	—	21.28 ± 0.36	11.00 ± 0.20	80.07
CS4	1.65	3840	0.290 (5)	0.268 (5)	66.46 ± 0.41	—	18.73 ± 0.23	14.40 ± 0.40	80.06
CS4	1.65	1400	0.403 (2)	0.377 (2)	64.32 ± 0.68	—	20.74 ± 0.17	14.40 ± 0.40	79.97
CS4	1.65	4215	0.500 (1)	0.473 (2)	64.36 ± 0.72	—	20.59 ± 0.36	14.40 ± 0.40	80.02
CS4	2	1260	0.305 (2)	0.277 (2)	63.96 ± 0.54	—	17.34 ± 0.18	18.25 ± 0.35	79.94
CS4	2	1330	0.493 (3)	0.460 (3)	62.78 ± 0.49	—	18.55 ± 0.13	18.25 ± 0.35	79.91
CS4A3	1	1060	0.297 (2)	0.283 (2)	70.00 ± 0.52	4.69 ± 0.25	19.12 ± 0.38	6.20 ± 0.25	79.92
CS4A3	1	1065	0.502 (2)	0.484 (2)	67.85 ± 0.51	5.01 ± 0.21	20.93 ± 0.44	6.20 ± 0.25	79.89
CS4A3	1.3	1740	0.294 (3)	0.276 (3)	67.27 ± 1.04	4.74 ± 0.23	17.70 ± 0.22	10.30 ± 0.05	79.98
CS4A3	1.3	1080	0.501 (1)	0.479 (1)	64.05 ± 0.54	5.39 ± 0.17	20.26 ± 0.12	10.30 ± 0.05	79.98
CS4A3	2	4170	0.290 (10)	0.265 (10)	62.97 ± 0.40	3.91 ± 0.06	16.02 ± 0.11	17.20 ± 0.45	79.91
CS4A3	2	1275	0.501 (1)	0.465 (2)	63.07 ± 0.79	4.00 ± 0.13	15.83 ± 0.20	17.20 ± 0.45	79.97
CS4A6	1	4140	0.306 (2)	0.292 (2)	69.71 ± 0.92	9.63 ± 0.12	15.01 ± 0.39	5.65 ± 0.25	79.98
CS4A6	1	1200	0.404 (2)	0.388 (2)	68.29 ± 0.41	9.81 ± 0.13	16.25 ± 0.19	5.65 ± 0.25	80.02
CS4A6	1	1080	0.501 (1)	0.484 (1)	66.90 ± 1.03	10.34 ± 0.47	17.10 ± 0.51	5.65 ± 0.25	80.07
CS4A6	1	1170	0.680 (1)	0.665 (1)	64.05 ± 0.43	11.36 ± 0.14	18.93 ± 0.22	5.65 ± 0.25	79.97
CS4A6	1.3	960	0.305 (2)	0.286 (2)	66.59 ± 0.54	8.99 ± 0.23	14.32 ± 0.17	10.10 ± 0.40	79.96
CS4A6	1.3	1260	0.406 (2)	0.385 (2)	65.27 ± 0.41	9.07 ± 0.11	15.57 ± 0.16	10.10 ± 0.40	80.03
CS4A6	1.3	1410	0.493 (3)	0.471 (3)	63.20 ± 0.89	9.17 ± 0.12	17.53 ± 0.45	10.10 ± 0.40	80.1
CS4A6	1.3	4140	0.700 (2)	0.681 (2)	61.24 ± 0.96	10.32 ± 0.24	18.34 ± 0.23	10.10 ± 0.40	79.9
CS4A6	1.65	1380	0.311 (2)	0.291 (2)	64.59 ± 0.40	8.28 ± 0.16	13.83 ± 0.37	13.30 ± 0.45	79.9
CS4A6	1.65	2670	0.409 (1)	0.386 (2)	62.71 ± 0.43	8.96 ± 0.15	15.03 ± 0.19	13.30 ± 0.45	79.9
CS4A6	1.65	1095	0.499 (3)	0.474 (3)	61.81 ± 0.35	9.31 ± 0.20	15.58 ± 0.26	13.30 ± 0.45	79.97
CS4A6	2	1070	0.311 (2)	0.283 (2)	61.25 ± 0.55	8.52 ± 0.19	13.52 ± 0.09	16.70 ± 0.45	79.94
CS4A6	2	1320	0.501 (1)	0.467 (2)	59.48 ± 0.80	9.56 ± 0.11	14.36 ± 0.28	16.70 ± 0.45	79.98

[a] $X_{H2}O$ = weight fraction of H_2O added to silicate in sample container. Numbers in parentheses represent error in last decimal. X_f = weight fraction of aqueous fluid at equilibrium during an experiment calculated from measured H_2O and silicate solubility in coexisting silicate melt and aqueous fluid (Mysen, 2002a,b) from Eqn. 1. Numbers in parentheses represent error in last decimal. H_2O = solubility in silicate melts from Mysen (2002a). $LiBO_2$ = wt% mixed with dehydrated quenched silicate melts before electron microprobe analysis of glasses (see text for detailed discussion).

quenched glass. In this calculation, the proportion of coexisting H_2O-saturated silicate melt and silicate-saturated aqueous fluid at equilibrium at high pressure and temperature was derived from the proportion of silicate and H_2O in the starting materials and the H_2O- and silicate-solubility in melt and fluid, respectively (solubility data from Mysen, 2002a,b). The actual weight fraction of aqueous fluid in equilibrium with melt, X_f, is related to the weight fraction of fluid in the starting composition, $X_{H2}O$, as follows:

$$X_f = \frac{\left(\frac{X_{H_2O}}{1 - X_{H_2O}}\right)\left(\frac{1 - X_{H_2O}^{melt}}{1 - X_{silicate}^{fluid}}\right)}{1 + \left(\frac{X_{H_2O}}{1 - X_{H_2O}}\right)\left(\frac{1 - X_{H_2O}^{melt}}{1 - X_{silicate}^{fluid}}\right)}, \quad (1)$$

where $X_{H_2O}^{melt}$ and $X_{silicate}^{fluid}$ are the solubility of H_2O in melt and of silicate in coexisting aqueous fluid as weight fractions.

The uncertainty in analyzed melt compositions is the standard error of the average of 10 analytical points per sample. The reported uncertainty is the standard error ($\pm 1\sigma$) of this average after recalculation of melt composition to a $LiBO_2$-free basis. The weighing error associated with mixing $LiBO_2$ with dehydrated silicate glass is ± 0.02 mg of actual weight. The errors in calculated aqueous fluid composition were calculated by progression of all weighing errors, errors in the analyzed melt composition, and published errors in H_2O contents of H_2O-saturated melts (Mysen, 2002a) and silicate-saturated aqueous fluids (Mysen, 2002b). As can be seen from the results (Tables 2A and 2B), these errors range from several tens of percent for the lowest-pressure experiments (lowest silicate content of fluid) to $<5\%$ for the most silicate-rich compositions.

The experimental run durations were $\sim$20 h or longer. In light of time studies conducted with similar experimental designs in the systems K_2O-Al_2O_3-SiO_2-H_2O and Na_2O-Al_2O_3-SiO_2-H_2O (Mysen and Armstrong, 2002), these experimental durations are more than adequate to reach equilibrium.

3. RESULTS AND DISCUSSION

3.1. Silicate Solution Behavior

Experimental results are summarized in Table 2A and 2B. The melt and fluid compositions (with errors) were obtained as discussed above. The H_2O contents of silicate melts and aqueous fluids are from Mysen (2002a,b). The $LiBO_2$ added to anhydrous glasses before electron microprobe analysis is also shown. The analytical data are, however, recalculated on a $LiBO_2$-free basis.

Table 2B. Experimental results: Calculated fluid compositions (wt%) and fluid/melt partition coefficients (oxide).[a]

Composition	Pressure (GPa)	Time (min)	SiO_2	Al_2O_3	CaO	H_2O
CS4	1	1185	0.496 ± 0.166	—	0.104 ± 0.035	99.40 ± 0.20
CS4	1	1230	0.505 ± 0.168	—	0.093 ± 0.031	99.40 ± 0.20
CS4	1	1215	0.513 ± 0.172	—	0.088 ± 0.029	99.40 ± 0.20
CS4	1.3	1410	1.846 ± 0.414	—	0.424 ± 0.096	97.75 ± 0.25
CS4	1.3	1200	1.901 ± 0.424	—	0.339 ± 0.076	97.75 ± 0.25
CS4	1.3	3060	1.859 ± 0.414	—	0.393 ± 0.088	97.75 ± 0.25
CS4	1.65	3840	3.584 ± 0.455	—	0.787 ± 0.106	95.60 ± 0.30
CS4	1.65	1400	3.717 ± 0.469	—	0.667 ± 0.086	95.60 ± 0.30
CS4	1.65	4215	3.631 ± 0.456	—	0.757 ± 0.098	95.60 ± 0.30
CS4	2	1260	5.345 ± 0.463	—	1.323 ± 0.120	93.30 ± 0.50
CS4	2	1330	5.417 ± 0.450	—	1.246 ± 0.105	93.30 ± 0.50
CS4A3	1	1060	0.391 ± 0.391	0.019 ± 0.019	0.090 ± 0.090	99.50 ± 0.25
CS4A3	1	1065	0.395 ± 0.396	0.020 ± 0.020	0.085 ± 0.085	99.50 ± 0.25
CS4A3	1.3	1740	1.313 ± 0.395	0.053 ± 0.021	0.334 ± 0.100	98.30 ± 0.25
CS4A3	1.3	1080	1.363 ± 0.403	0.055 ± 0.017	0.282 ± 0.083	98.30 ± 0.25
CS4A3	2	4170	3.322 ± 0.531	0.204 ± 0.039	0.924 ± 0.145	95.55 ± 0.45
CS4A3	2	1275	3.341 ± 0.515	0.201 ± 0.034	0.908 ± 0.139	95.55 ± 0.45
CS4A6	1	4140	0.389 ± 0.302	0.036 ± 0.028	0.075 ± 0.058	99.50 ± 0.15
CS4A6	1	1200	0.396 ± 0.307	0.039 ± 0.030	0.065 ± 0.051	99.50 ± 0.15
CS4A6	1	1080	0.397 ± 0.308	0.038 ± 0.030	0.065 ± 0.050	99.50 ± 0.15
CS4A6	1	1170	0.393 ± 0.305	0.040 ± 0.031	0.067 ± 0.052	99.50 ± 0.15
CS4A6	1.3	960	1.161 ± 0.348	0.116 ± 0.037	0.223 ± 0.067	98.50 ± 0.20
CS4A6	1.3	1260	1.184 ± 0.354	0.123 ± 0.037	0.194 ± 0.058	98.50 ± 0.20
CS4A6	1.3	1410	1.205 ± 0.360	0.092 ± 0.028	0.203 ± 0.061	98.50 ± 0.20
CS4A6	1.3	4140	1.203 ± 0.359	0.111 ± 0.033	0.186 ± 0.056	98.50 ± 0.20
CS4A6	1.65	1380	1.984 ± 0.516	0.231 ± 0.062	0.385 ± 0.104	97.40 ± 0.45
CS4A6	1.65	2670	2.062 ± 0.534	0.203 ± 0.054	0.335 ± 0.088	97.40 ± 0.45
CS4A6	1.65	1095	2.058 ± 0.532	0.203 ± 0.053	0.338 ± 0.088	97.40 ± 0.45
CS4A6	2	1070	3.389 ± 0.480	0.307 ± 0.053	0.604 ± 0.088	95.70 ± 0.35
CS4A6	2	1320	3.566 ± 0.498	0.272 ± 0.039	0.552 ± 0.078	95.70 ± 0.35

[a] Results are ordered as in Table 2.

The composition of coexisting silicate melts and aqueous fluid at 1–2 GPa and 1200°C, recalculated on an anhydrous basis, is shown in Figure 1. Similar data from the system Na_2O-Al_2O_3-SiO_2-H_2O in the same pressure range, but at 1100°C (data from Mysen and Armstrong, 2002), are also shown in Figure 1.

The proportions of CaO, Al_2O_3, and SiO_2 in coexisting silicate melt and aqueous fluid, recalculated to an anhydrous basis, differ (Fig. 1). It is clear, therefore, that at least in the 1–2 GPa pressure range and 1200°C, the solubility behavior in both aqueous fluid and silicate melt is incongruent. Incongruent solubility of alkali aluminosilicate components in aqueous fluids were also observed for the equivalent compositions in the systems Na_2O-Al_2O_3-SiO_2-H_2O and K_2O-Al_2O_3-SiO_2-H_2O (NS4, NS4A3, NS4A6, KS4, KS4A3, and KS4A6) in the same pressure range and at 1100°C (Mysen and Armstrong, 2002; see also fig. 1, for example, of their data from the Na_2O-Al_2O_3-SiO_2-H_2O system). Incongruent solubility of components of the $NaAlSi_3O_8$ composition was reported by Stalder et al. (2000) for similar pressures but at lower temperatures.

The element fractionation between fluid and melt in alkali and alkaline earth (Ca) aluminosilicate systems differs in detail. In the Na_2O-Al_2O_3-SiO_2-H_2O and K_2O-Al_2O_3-SiO_2-H_2O systems, on an anhydrous basis, aqueous fluid is depleted in SiO_2 relative to melt, whereas alkalis are enriched (Fig. 1). The reverse case for SiO_2 is observed for the system CaO-Al_2O_3-SiO_2-H_2O, where there is a relative enrichment of SiO_2 in the aqueous fluid and a depletion in CaO (Fig. 1). In both groups of systems, Al_2O_3 is depleted in the aqueous fluid relative to the melt. The extent of Al_2O_3 depletion is greater in the CaO-Al_2O_3-SiO_2-H_2O system compared with both the Na_2O-Al_2O_3-SiO_2-H_2O and K_2O-Al_2O_3-SiO_2-H_2O systems (Mysen and Armstrong, 2002; see also Fig. 1).

The results summarized in Figure 1 include data not only for different pressures (1, 1.3, 1.5, 1.65, and 2.0 GPa) but also from experiments where the proportion of aqueous fluid relative to silicate melts (X_f; see Eqn. 1) varied. This proportion, X_f, was employed as a variable to examine the extent of incongruent solution behavior of Ca, Al, and Si in coexisting melt and fluid. If the solution behavior were congruent, the concentration of the individual oxides in fluid and melt would be independent of X_f, whereas with incongruent solution, the oxide concentrations depend on X_f.

For the three compositions in the CaO-Al_2O_3-SiO_2-H_2O system (CS4, CS4A3, and CS4A6), the SiO_2 content of the H_2O-satured melts increases with decreasing weight fraction of H_2O in the experimental charge. The SiO_2 content of coexisting silicate-saturated aqueous fluid decreases. For CaO, the relationship between CaO content and fluid fraction, X_f, is the inverse (Fig. 2). The relationships between Al_2O_3 contents of X_f follow the same trend as those of CaO in silicate melt and aqueous fluid. These variations on oxide concentration with fluid fraction indicate incongruent solution in aqueous fluid in the CaO-Al_2O_3-SiO_2-H_2O. Solution in coexisting melt, therefore, is also incongruent.

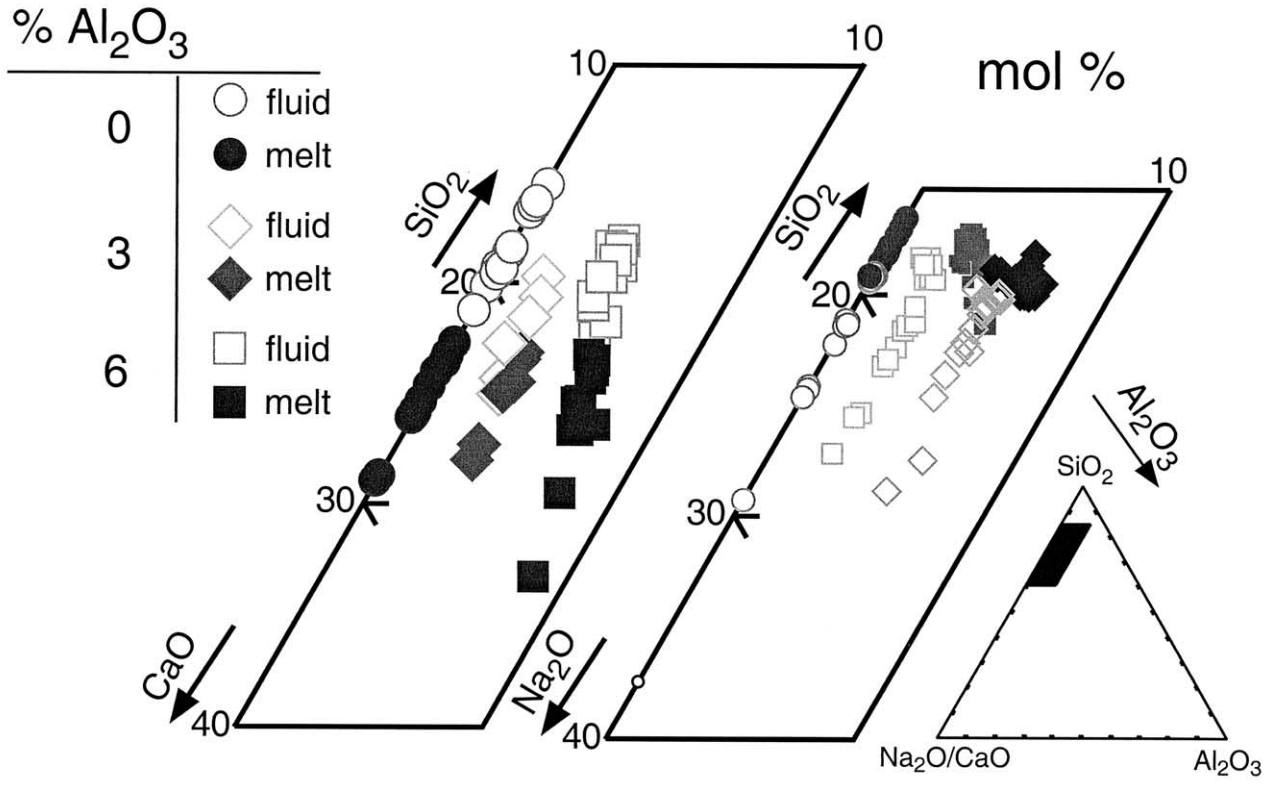

Fig. 1. Composition of coexisting silicate melt and aqueous fluid recalculated on an anhydrous basis. Data from the system Na_2O-Al_2-SiO_2-H_2O from Mysen and Armstrong (2002).

3.2. Fluid/Melt Partitioning

Because of the incongruent nature of the oxide solution in silicate melts and aqueous fluids, fluid/melt partition coefficients depend on the fluid/melt ratio (X_f) in the experimental charges. To estimate the fluid/melt partition coefficient at the H_2O-saturation value in the silicate melts (data from Mysen, 2002b, and indicated with vertical lines marked as x(1), x(1.3), x(1.65) and x(2.0) in Fig. 2), the oxide concentrations in fluid and melts from Fig. 2 were extrapolated until intersection with the H_2O-saturation in the melts at each pressure. A simple straight line satisfies the data. There is no intrinsic reason why the data in Figure 2 should be described with a straight line. However, within the uncertainty of the experimental results, a straight line often is sufficient to describe the relationships between oxide concentration and weight fraction of aqueous fluid in the experimental charges and this simple form was used here whenever possible. The errors in these partition coefficients reflect errors in these straight-line fits.

Partition coefficients, $D_{oxide}^{fluid/melt}$, are shown for SiO_2, Al_2O_3, and CaO in Figure 3 (solid symbols) and compared with $D_{oxide}^{fluid/melt}$ results for SiO_2, Al_2O_3, and Na_2O for compositions NS4, NS4A3, and NS4A6 from the system Na_2O-Al_2O_3-SiO_2-H_2O (open symbols) (data from Mysen and Armstrong, 2002). The $D_{oxide}^{fluid/melt}$ data for equivalent compositions, KS4, KS4A3, and KS4A6, in the system K_2O-Al_2O_3-SiO_2-H_2O (Mysen and Armstrong, 2002) resemble those of NS4, NS4A3, and NS4A6 and are not shown.

The fluid/melt partition coefficients for CaO, Al_2O_3, and SiO_2 range between ~0.002 and 0.04 and increase by a factor of 4–5 between 1 and 2 GPa (Fig. 3). At all pressures and for all three starting compositions, in the system CaO-Al_2O_3-SiO_2-H_2O $D_{CaO}^{fluid/melt} > D_{SiO2}^{fluid/melt} \gg D_{Al2O3}^{fluid/melt}$. The D-values for Al_2O_3 and SiO_2 are between 10 and 20% of those determined for the NS4, NS4A3, and NS4A6 compositions (Mysen and Armstrong, 2002; see also Fig. 3). The $D_{Na2O}^{fluid/melt}$ is more than an order of magnitude greater than $D_{CaO}^{fluid/melt}$.

The difference between $Al_2O_3^{fluid/melt}$ and the partition coefficients for CaO and SiO_2 diminishes with increasing pressure. This latter effect is more pronounced for the fluid/melt pairs in the CaO-Al_2O_3-SiO_2-H_2O system than for the equivalent pairs in the Na_2O-Al_2O_3-SiO_2-H_2O and K_2O-Al_2O_3-SiO_2-H_2O systems (Mysen and Armstrong, 2002; see also Fig. 3). The $D_{oxide}^{fluid/melt}$-value at the X_f-values corresponding to H_2O-saturation in the silicate melt at given pressure decreases with increasing Al_2O_3 of the starting material, as was also observed for the $D_{oxide}^{fluid/melt}$ for the equivalent compositions in the Na_2O-Al_2O_3-SiO_2-H_2O and K_2O-Al_2O_3-SiO_2-H_2O systems (Table 3).

The relationships between the composition of the starting materials and fluid/melt partition coefficients lead to the suggestion that the oxides in question may form complexes in the coexisting fluids and melt and that the type of complexing affects their solution behavior. Relationships between fluid composition and $D_{oxide}^{fluid/melt}$ are depicted in Figure 4 with

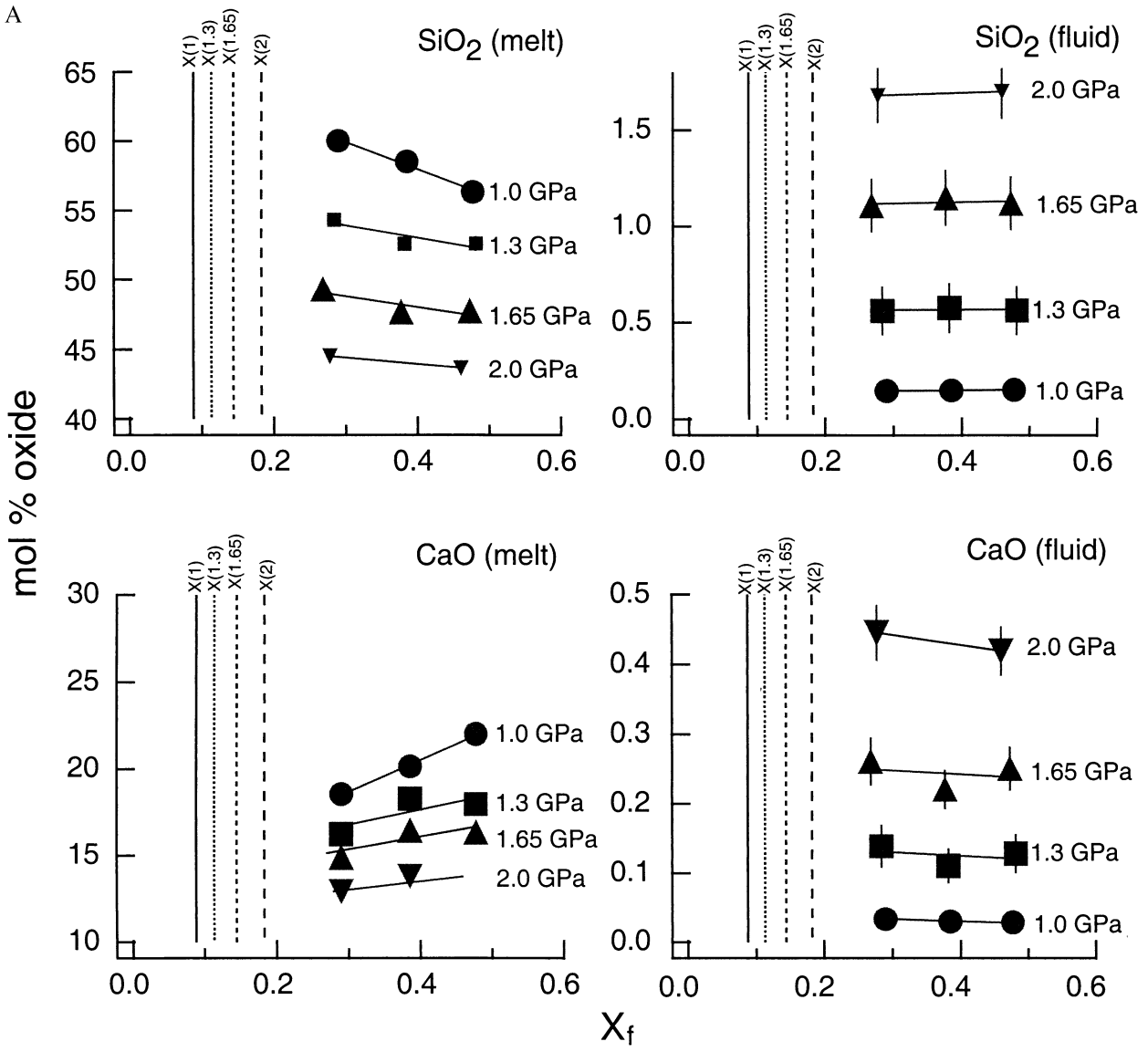

Fig. 2A. Composition coexisting silicate melt and aqueous fluid as a function of proportion of fluid, X_f, at pressures indicated. (A) Results from starting composition, CS4.

results of regression analysis of these data in Table 4. In this analysis, data from the systems Na_2O-Al_2O_3-SiO_2-H_2O and K_2O-Al_2O_3-SiO_2-H_2O (Mysen and Armstrong, 2002) were also included.

There is a positive correlation between $D_{SiO2}^{fluid/melt}$ and alkali, alkaline earth, and alumina concentration in the fluid (Fig. 4A). The rate of change of $D_{SiO2}^{fluid/melt}$ with K_2O, Na_2O, and CaO concentration in the fluid is approximately the same ($\sim$0.09–0.16 mol%$^{-1}$), whereas the influence of Al_2O_3 on $D_{SiO2}^{fluid/melt}$ depends on whether the metal cation is an alkali metal (Na and K) or alkaline earth (Ca) (Table 4). The rate of change of $D_{SiO2}^{fluid/melt}$ with CaO concentration in the CaO-Al_2O_3-SiO_2-H_2O system is only 25–35% of that between $D_{SiO2}^{fluid/melt}$ and Na_2O and K_2O in the Na_2O-Al_2O_3-SiO_2-H_2O and K_2O-Al_2O_3-SiO_2-H_2O systems, respectively (Table 4).

The $Al_2O_3^{fluid/melt}$ and $D_{K,Na,Ca}^{fluid/melt}$ also depend on fluid composition (Figs. 4B, C) with both sets of partition coefficients positively correlated with the SiO_2 content of the fluid. The $Al_2O_3^{fluid/melt}$ increases with alkali and alkaline earth content, and $D_{K,\ Na,\ Ca}^{fluid/melt}$ increases with increasing Al_2O_3 content of the fluid (Fig. 6, Table 4). The $Al_2O_3^{fluid/melt}$ is distinctly more sensitive to SiO_2 content in the Na_2O-Al_2O_3-SiO_2-H_2O and K_2O-Al_2O_3-SiO_2-H_2O systems than in the CaO-Al_2O_3-SiO_2-H_2O system. The rate of change of $Al_2O_3^{fluid/melt}$ in the latter system is only $\sim$10% of that in the systems Na_2O-Al_2O_3-SiO_2-H_2O and K_2O-Al_2O_3-SiO_2-H_2O (Table 4). This difference is similar to the difference between the rate of change of $D_{SiO2}^{fluid/melt}$ with Al_2O_3 content of the fluid in these three systems. The rate of change of $D_{CaO}^{fluid/melt}$ with Al_2O_3 content in the CaO-Al_2O_3-SiO_2-H_2O system is $\sim$10–30% of the rate of change of $D_K^{fluid/melt}$ and $D_{Na}^{fluid/melt}$ with Al_2O_3

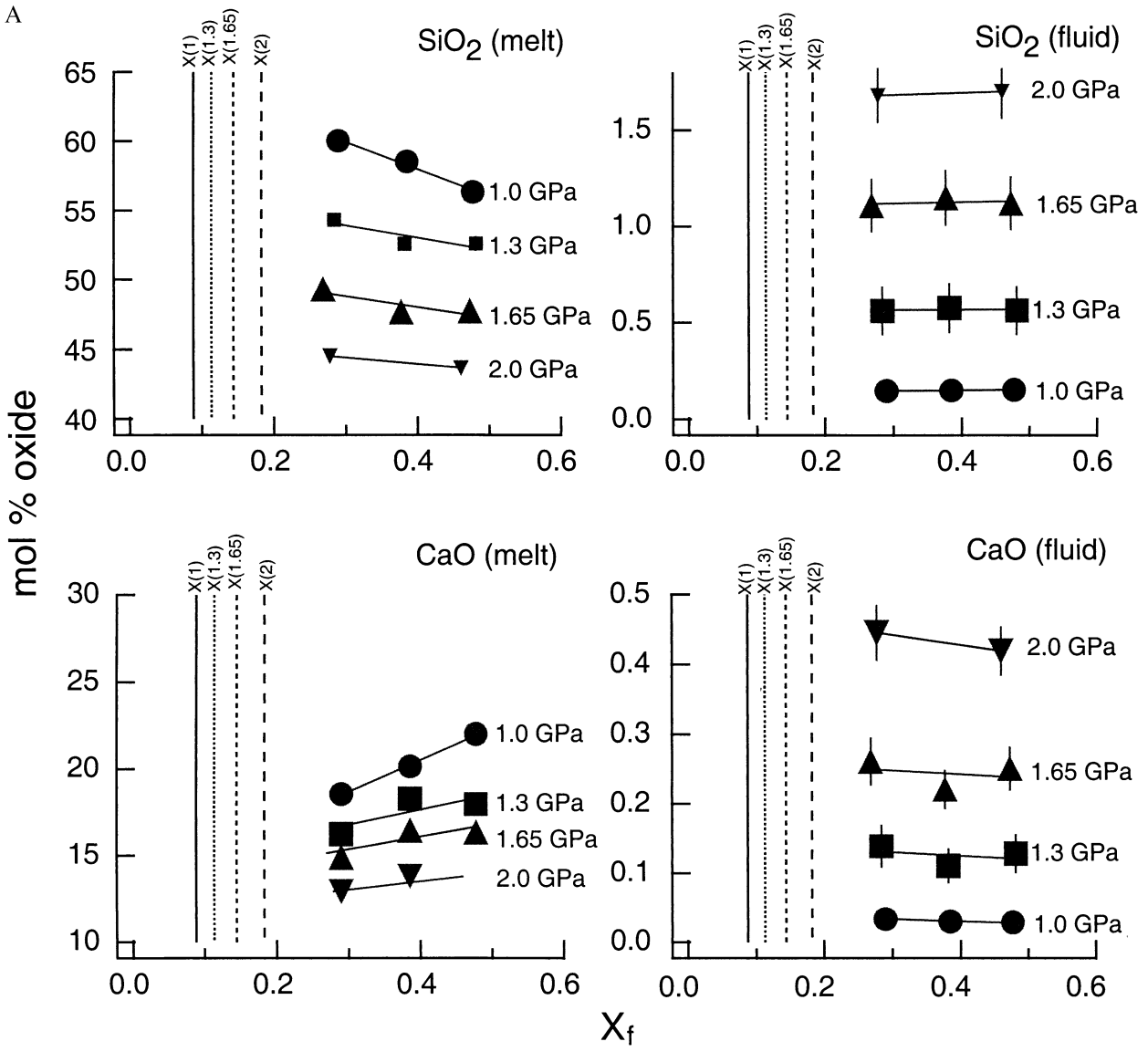

Fig. 2B. Composition coexisting silicate melt and aqueous fluid as a function of proportion of fluid, X_f, at pressures indicated. (B) Results from starting composition, CS4A3.

concentration in the Na_2O-Al_2O_3-SiO_2-H_2O and K_2O-Al_2O_3-SiO_2-H_2O systems.

Melt composition is also variable. Melt composition changes, however, are small compared with the relative changes in fluid composition and no clear relations between melt composition and $D_{oxide}^{fluid/melt}$ were observed.

The relations between $D_{oxide}^{fluid/melt}$ and fluid composition point to possible complexes in the fluids. These complexes include association between silicate polymers and alkalis or alkaline earths as well as possible aluminosilicate complexing. Zhang and Frantz (2000) and Newton and Manning (2002) suggested from their solubility experiments in the system MgO-SiO_2-H_2O that silicate species in aqueous fluids in the pressure/temperature regime under discussion may occur as various depolymerized species (e.g., SiO_4^{4-}, $Si_2O_7^{6-}$, and so forth). Those suggested complexes are consistent with Raman spectroscopic data obtained for silicate-saturated aqueous fluids where similar structural complexes were observed (Mysen, 1998; Zotov and Keppler, 2000, 2002). These silicate complexes may be associated with alkali metals (in addition to H^+ and possible H_2O solvation).

The positive correlation between $D_{K,\,Na,\,Ca}^{fluid/melt}$ and SiO_2 and between $D_{SiO2}^{fluid/melt}$ and K_2O, Na_2O, and CaO concentration in the aqueous fluid is consistent with a solution model where the silicate polymers are associated with alkalis or alkaline earths. Association among anions and cations is likely at these high temperatures because the dielectric constant for H_2O is quite low (e.g., Pitzer, 1983). Positive correlation between association constants and temperature has been reported for other salts dissolved in aqueous fluids at high temperature and pressure (e.g., Frantz and Marshall, 1984; Marshall and Frantz, 1987; Frantz et al., 1993). Association between metals and

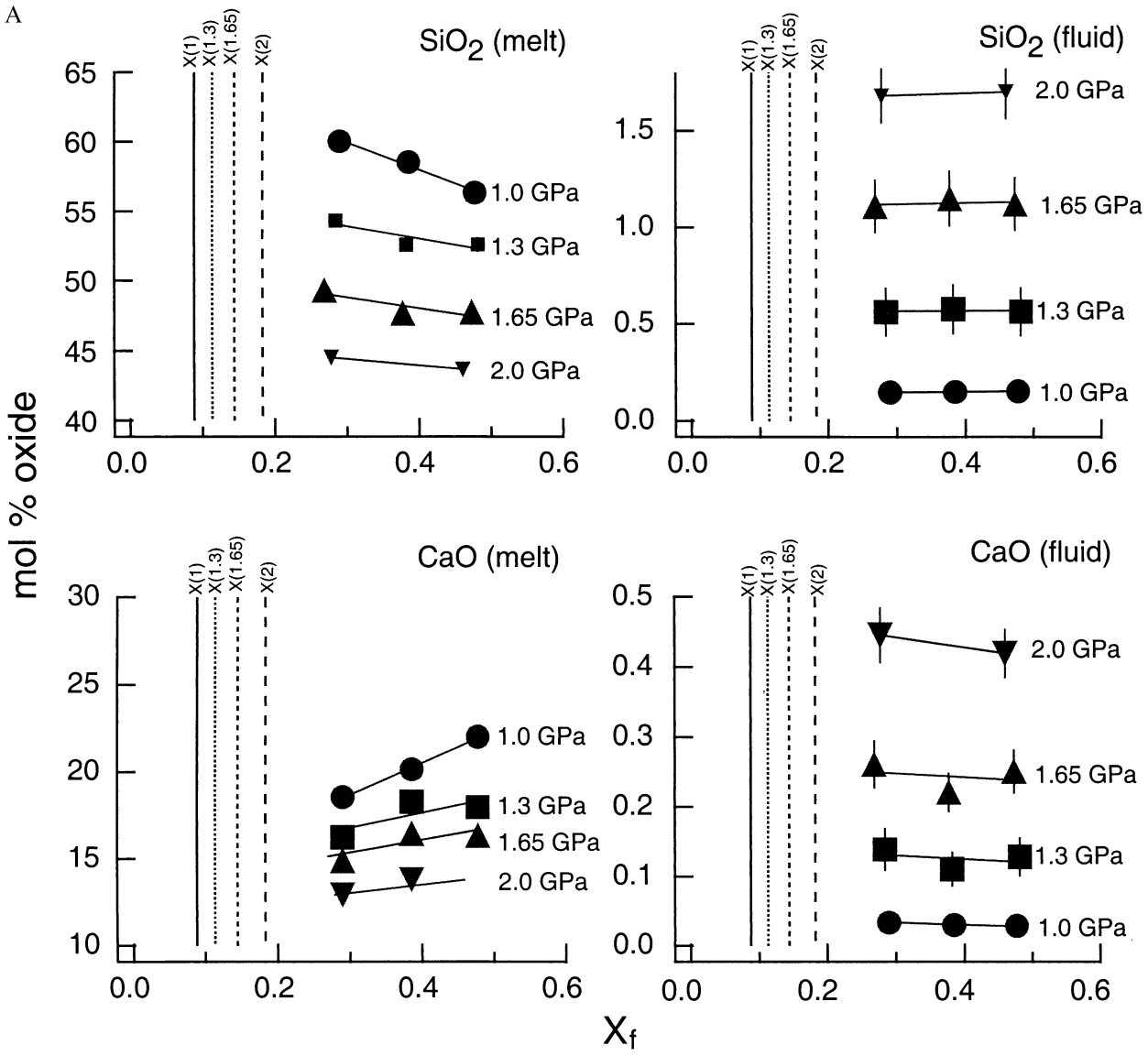

Fig. 2C. Composition coexisting silicate melt and aqueous fluid as a function of proportion of fluid, X_f, at pressures indicated. (C) Results from starting composition, CS4A6. x(1), x(1.3), x(1.65), and x(2) denote H_2O solubility in melt composition at pressure (GPa) indicated in parentheses (data from Mysen, 2002b).

silicate polymers may also be analogous to that observed spectroscopically in silicate melts (e.g., Jones et al., 2001).

The positive correlation between $Al_2O_3^{fluid/melt}$ and the concentration of K_2O, Na_2O, and CaO (Fig. 4B) and that between $D_{K,\,Na,\,Ca}^{fluid/melt}$ and Al_2O_3 concentration in the fluid (Fig. 4C) lead to the suggestion that Al_2O_3 is associated with alkali metals and alkaline earth in the aqueous fluids. One such association may be Al^{3+} in a tetrahedral complex with oxygen where tetrahedrally-coordinated Al^{3+} is charge-balanced with alkalis or alkaline earth. This concept is analogous to the well-established concept of alkali- and alkaline earth charge-balanced Al^{3+} in tetrahedrally-coordinated aluminate and aluminosilicate complexes in silicate melts and crystals (see, for example, Mysen, 1995, for review of such information). The observation that, on a molar basis, the rate of change of $Al_2O_3^{fluid/melt}$ with CaO concentration and the rate of change of $D_{CaO}^{fluid/melt}$ with Al_2O_3 concentration are both considerably smaller than the equivalent relationships involving alkali metals and Al_2O_3 (Table 4) leads to the suggestion that possible Ca-charge-balanced aluminate complexes are less stable than those involving alkali charge-balanced tetrahedrally coordinated Al^{3+} in aluminate complexes. Again using aluminosilicate melts as an analogy, that conclusion is consistent with thermodynamic and structural data for melts and glasses along aluminate-silica joins (see Mysen, 1988, for review of those data).

The positive correlation between $Al_2O_3^{fluid/melt}$ and SiO_2 concentration of fluid and between $D_{SiO2}^{fluid/melt}$ and Al_2O_3 concentration in the fluid (Figs. 4A, B; Table 4) suggests that in aqueous aluminosilicate fluids there may also be association

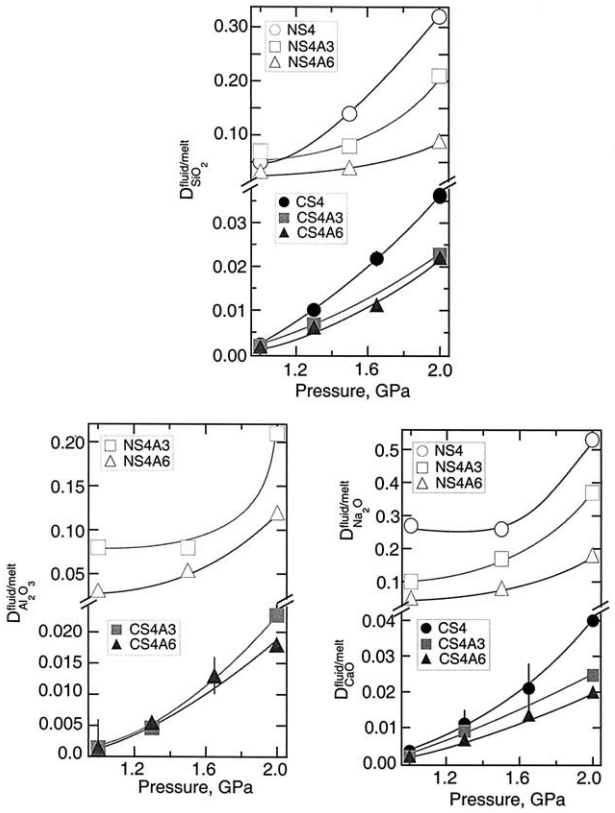

Fig. 3. Fluid/melt partition coefficients ($D_{oxide}^{fluid/melt}$) for SiO_2, Al_2O_3, and CaO in the system CaO-Al_2O_3-SiO_2-H_2O (closed symbols) and for SiO_2, Al_2O_3 and Na_2O in the system Na_2O-Al_2O_3-SiO_2-H_2O (open symbols, data from Mysen and Armstrong, 2002) as a function of pressure at the fluid + melt/melt boundary (corresponding to H_2O-saturation in melt for composition and pressure of interest). Error bars for partition coefficients in the system CaO-Al_2O_3-Sio_2-H_2O were calculated from the errors in the linear fits to the data in Figure 2. Error bars were not reported in the alkali aluminosilicate system.

between Si^{4+} and Al^{3+}. In other words, we suggest that alkali and alkaline earth aluminosilicate complexes, possibly with Al^{3+} and Si^{4+} in tetrahedral coordination with oxygen, exist in aqueous fluids in the high temperature- and high pressure-range under study. The extent to which H^+ and H_2O molecules (H_2O solvation?) are incorporated in these suggested complexes cannot be ascertained with the present data. The less pronounced correlations among these variables in the CaO-Al_2O_3-SiO_2-H_2O system compared with those in the systems Na_2O-Al_2O_3-SiO_2-H_2O and K_2O-Al_2O_3-SiO_2-H_2O are consistent with a suggestion that among these aluminosilicate complexes, Ca-aluminosilicate complexes are less stable than Na- and K-aluminosilicate complexes.

4. CONCLUDING REMARKS

From experimental data in the systems Na_2O-Al_2O_3-SiO_2-H_2O, K_2O-Al_2O_3-SiO_2-H_2O, and CaO-Al_2O_3-SiO_2-H_2O, we find that the solution behavior of the individual oxides in coexisting H_2O-saturated silicate melts and silicate-saturated aqueous fluids is incongruent. The aqueous fluids are depleted in alumina relative to silicate melt. There is a difference between the K_2O, Na_2O, and CaO behavior in that in the CaO-Al_2O_3-SiO_2-H_2O system, recalculated to an anhydrous basis $CaO^{fluid}/CaO^{melt} < 1$, whereas in the Na_2O-Al_2O_3-SiO_2-H_2O and K_2O-Al_2O_3-SiO_2-H_2O systems, K_2O^{fluid}/K_2O^{melt} and $Na_2O^{fluid}/Na_2O^{melt}$ both exceed unity.

In the Na_2O-Al_2O_3-SiO_2-H_2O, K_2O-Al_2O_3-SiO_2-H_2O, and CaO-Al_2O_3-SiO_2-H_2O systems, fluid/melt partition coefficients for the individual oxides range between ~0.005 and 0.35 depending on composition and pressure. The alkali partition coefficients are ~1 order of magnitude higher than that of CaO. Alumina and silica partition coefficient values in the CaO-Al_2O_3-SiO_2-H_2O system are less than 10–20% of the values for the same oxides in the Na_2O-Al_2O_3-SiO_2-H_2O and K_2O-Al_2O_3-SiO_2-H_2O systems.

Table 3. Relative effect of Al_2O_3 (% relative to Al-free composition) on fluid/melt partition coefficients, D, of SiO_2, K_2O, Na_2O, and CaO in the systems K_2O-Al_2O_3-SiO_2 (KAS),[a] Na_2O-Al_2O_3-SiO_2 (NAS)[a], and CaO-Al_2O_3-SiO_2 (CAS) as a function of pressure at 1200°C.

	D_{SiO2}^{KAS}		
Pressure, GPa	KS4	KS4A3	KS4A6
1	100	75	29
1.5	100	76	36
2	100	105	47
	D_{SiO2}^{NAS}		
Pressure, GPa	NS4	NS4A3	NS4A6
1	100	95	60
1.5	100	57	29
2	100	65	28
	D_{SiO2}^{CAS}		
Pressure, GPa	CS4	CS4A3	CS4A6
1	100	88	81
1.3	100	67	61
2	100	63	61
	D_{K2O}^{KAS}		
Pressure, GPa	KS4	KS4A3	KS4A6
1	100	46	18
1.5	100	27	21
2	100	45	50
	D_{Na2O}^{NAS}		
Pressure, GPa	NS4	NS4A3	NS4A6
1	100	37	19
1.5	100	65	31
2	100	70	34
	D_{CaO}^{CAS}		
Pressure, GPa	CS4	CS4A3	CS4A6
1	100	57	60
1.3	100	82	60
2	100	62	60

[a] Data from Mysen and Armstrong (2002), where symbols NS4, NS4A3, NS4A6, KS4, KS4A3, and KS4A6 refer to compositions in the NAS and KAS systems equivalent to CS4, CS4A3, and CS4A6 in the CAS system. The oxide concentrations are those calculated from the analytical data combined with H_2O- and silicate-solubility data from coexisting melt and aqueous fluids, respectively (Mysen, 2002a,b).

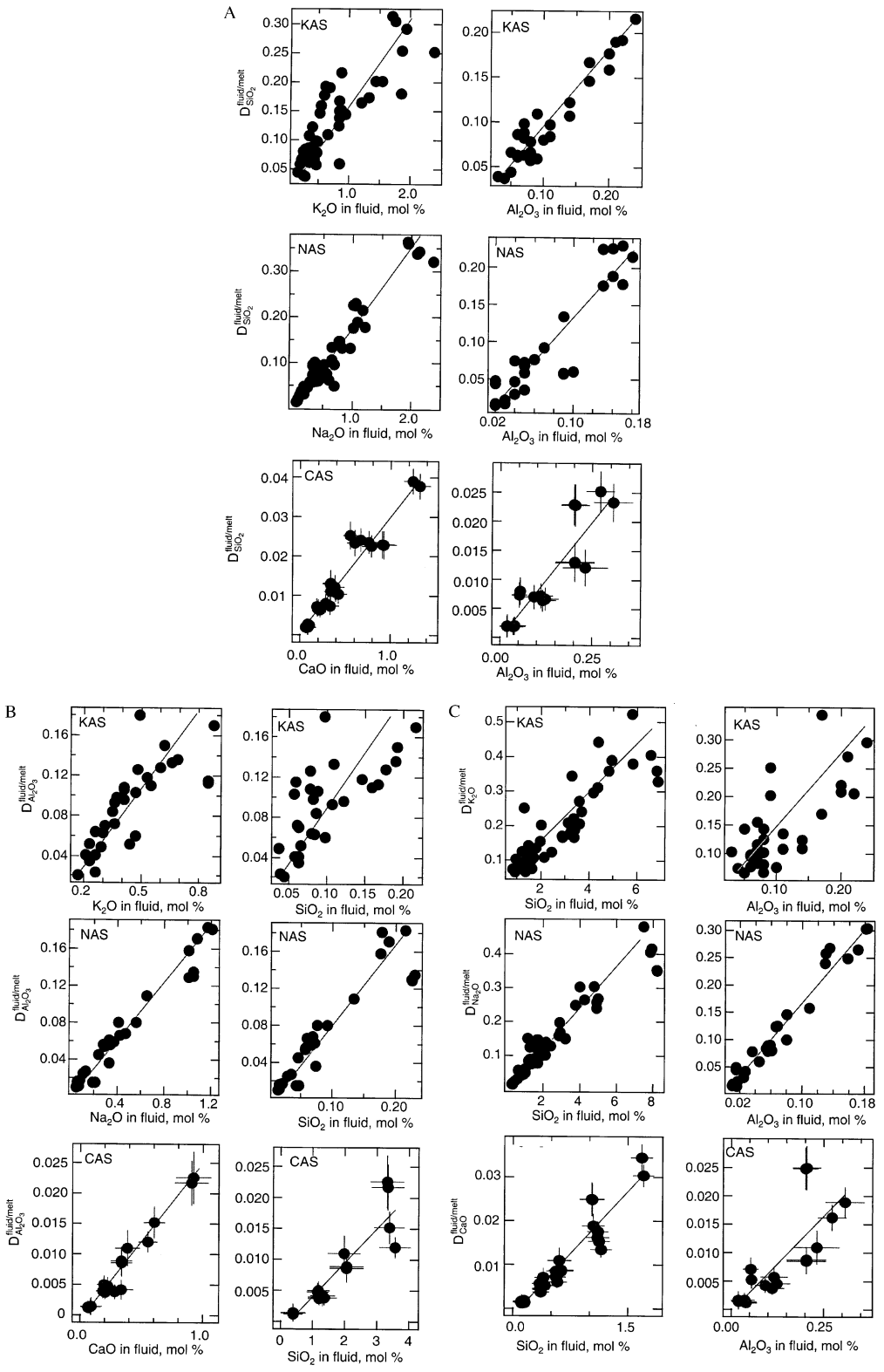

Fig. 4. Fluid/melt partition coefficients ($D_{oxide}^{fluid/melt}$) for SiO_2, Al_2O_3, and CaO, Na_2O, and K_2O in the systems CaO-Al_2O_3-SiO_2-H_2O (CAS), Na_2O-Al_2O_3-SiO_2-H_2O (NAS) (data from Mysen and Armstrong, 2002), and K_2O-Al_2O_3-SiO_2-H_2O (KAS) (data from Mysen and Armstrong, 2002) as a function of oxide concentration in silicate-saturated aqueous fluid. (A) Relations between $D_{SiO2}^{fluid/melt}$ and oxides. (B) Relations between $D_{Al_2O_3}^{fluid/melt}$ and oxides. (C) Relations between $D_{K2}O^{fluid/melt}$ and oxides, $D_{Na2}O^{fluid/melt}$ and oxides, and $D_{CaO}^{fluid/melt}$ and oxides. For discussion or error bars, see Figure 3 and text.

Positive correlations among individual partition coefficients and oxide concentrations in the aqueous fluids are consistent with complexing in the fluid that involves silicate polymers and alkalis and alkaline earths and aluminosilicate complexes where alkalis and alkaline earths may serve to charge-balance Al^{3+} in, perhaps tetrahedral coordination. The alkali alumino-

Table 4. Regression coefficients for the straight line fits in Fig. 5 [$D_{oxide}^{fluid/melt} = a + b \cdot C_{oxide(1)}(mol\%)$].

Partition coefficient	Oxide(1)	a	b	R^2
$D_{K2O}^{fluid/melt}$	SiO_2(KAS)[a]	0.02 (2)	0.061 (5)	0.78
$D_{Na2O}^{fluid/melt}$	SiO_2(NAS)[a]	0.019 (2)	0.050 (2)	0.92
$D_{CaO}^{fluid/melt}$	SiO_2(CAS)	−0.002 (1)	0.019 (1)	0.95
$D_{K2O}^{fluid/melt}$	Al_2O_3(KAS)	0.05 (2)	0.9 (2)	0.55
$D_{Na2O}^{fluid/melt}$	Al_2O_3(NAS)	−0.001 (6)	1.68 (7)	0.96
$D_{CaO}^{fluid/melt}$	Al_2O_3(CAS)	−0.001 (19)	0.07 (1)	0.80
$D_{SiO2}^{fluid/melt}$	K_2O(KAS)	0.046 (9)	0.11 (1)	0.74
$D_{SiO2}^{fluid/melt}$	Na_2O(NAS)	0.013 (5)	0.158 (6)	0.93
$D_{SiO2}^{fluid/melt}$	CaO(CAS)	0.0005 (8)	0.029 (1)	0.97
$D_{SiO2}^{fluid/melt}$	Al_2O_3(KAS)	0.012 (5)	0.80 (8)	0.92
$D_{SiO2}^{fluid/melt}$	Al_2O_3(NAS)	−0.01 (1)	1.4 (1)	0.84
$D_{SiO2}^{fluid/melt}$	Al_2O_3(CAS)	−0.0006 (14)	0.008 (9)	0.91
$D_{Al2O3}^{fluid/melt}$	K_2O(KAS)	0.02 (1)	0.17 (3)	0.61
$D_{Al2O3}^{fluid/melt}$	Na_2O(NAS)	0.005 (4)	0.140 (6)	0.96
$D_{Al2O3}^{fluid/melt}$	CaO(CAS)	−0.0007 (5)	0.025 (9)	0.98
$D_{Al2O3}^{fluid/melt}$	SiO_2(KAS)	0.03 (1)	0.6 (1)	0.52
$D_{Al2O3}^{fluid/melt}$	SiO_2(NAS)	0.008 (7)	0.71 (6)	0.86
$D_{Al2O3}^{fluid/melt}$	SiO_2(CAS)	−0.002 (1)	0.055 (5)	0.93

[a] Data from the systems KAS (K_2O-Al_2O_3-SiO_2) and NAS (Na_2O-Al_2O_3-SiO_2) from Mysen and Armstrong (2002). The oxide concentrations are those calculated from the analytical data combined with H_2O- and silicate-solubility data from coexisting melt and aqueous fluids, respectively (Mysen, 2002a,b).

silicate complexes appear more stable than Ca-aluminosilicate complexes.

Acknowledgments—This research was partially supported by the Summer Intern Program of the Carnegie Institution of Washington, which is gratefully acknowledged. This research was partially supported by NSF grant EAR-9901886.

Associate editor: C. Romano

REFERENCES

Aoki K. (1987) Japanese island arcs: Xenoliths in alkali basalts, high-alumina basalts, and calc-alkaline andesites and dacites. In *Mantle Xenoliths* (ed. P. H. Nixon), pp. 319–333. Wiley.

Bebout G., Ryan J. G., and Leeman W. P. (1993) B-Be systematics in subduction-related metamorphic rocks; characterization of the subducted component. *Geochim. Cosmochim. Acta* **57**, 2227–2237.

Bohlen S. R. (1984) Equilibria for precise pressure calibration and a frictionless furnace assembly for the piston-cylinder apparatus. *N. Jb. Mineral. Mh.* **84** (9), 404–412.

Boyd F. R. and England J. L. (1960) Apparatus for phase equilibrium measurements at pressures up to 50 kilobars and temperatures up to 1750°C. *J. Geophys. Res.* **65**, 741–748.

Brenan J. M., Shaw H. F., Ryerson F. J., and Phinney D. L. (1995) Mineral-aqueous fluid partitioning of trace elements at 900° and 2.0GPa: Constraints on the trace element geochemistry of mantle and deep crustal fluids. *Geochim. Cosmochim. Acta* **59**, 3331–3350.

Brenan J. M., Ryerson F. J., and Shaw H. F. (1998) The role of aqueous fluids in the slab-to-mantle transfer of boron, beryllium, and lithium during subduction: Experiments and models. *Geochim. Cosmochim. Acta* **62**, 3337–3348.

Ernst W. G., Mosenfelder J. L., Leech M. L., and Liu J. G. (1998) H_2O recycling during continental collision: Phase-equilibrium and kinetic considerations. In *When Continents Collide: Geodynamics and Geochemistry of Ultrahigh-Pressure Rocks* (ed. J. G. Liu), pp. 275–296. Kluwer Academic.

Foley S. F., Jackson S. E., Fryer B. J., Greenough J. D., and Jenner G. A. (1996) Trace element partition coefficients for clinopyroxene and phlogopite in an alkaline lamprophyre from, Newfoundland by LAM-ICP-MS. *Geochim. Cosmochim. Acta* **60**, 629–638.

Fowler M. B. (1984) Large-ion lithophile element mobility in the lower continental crust: Mineralogy and geochemistry of the hornblende-granulite subfacies at Gruinard Bay and its relationships with amphibolite-facies and granulite-facies end members. In *Metamorphic Studies: Research in Progress.*, Vol. 141 (ed. M. Brown), pp. 1076. Geological Society of London.

Frantz J. D. and Marshall W. L. (1984) Electrical conductances and ionization constants of salts, acids, and bases in supercritical aqueous fluids. I. Hydrochloric acid from 150° to 700°C and pressures to 4000 bars. *Am. J. Sci.* **284**, 651–667.

Frantz J. D., Dubessy J., and Mysen B. O. (1993) An optical cell for Raman spectroscopic studies of supercritical fluids and its applications to the study of water to 500 °c and 2000 bar. *Chem. Geol.* **106**, 9–26.

Getting I. C. and Kennedy G. C. (1970) Effect of pressure on the emf of chromel-alumel and platinum-platinum 90 rhodium 10 thermocouples. *J. Appl. Phys.* **11**, 4552–4562.

Iizuka Y. and Nakamura E. (1995) Experimental study of the slab-mantle interaction and implications for the formation of titanoclinohumite at deep subduction zone. *Proc. Japan Acad.* **71**, 159–164.

Iizuka Y. and Mysen B. O. (1998) Experimental study on dehydration and silica metasomatism in the subduction zones. *Terra Nova* **10** (1), 28.

Ionov D. A. and Hofmann A. W. (1995) Nb-Ta-rich mantle amphiboles and micas. Implications for subduction-related metasomatic trace element fractionations. *Earth Planet. Sci. Lett.* **131**, 341–356.

Jones A. R., Winter R., Greaves G. N., and Smith I. H. (2001) MAS NMR study of soda-lime-silicate glasses with variable degrees of polymerisation. *J. Non-Cryst. Solids* **293**, 87–92 –295.

Konzett J. and Ulmer P. (1999) The stability of hydrous potassic phases in lherzolitic mantle—An experimental study to 9.5 GPa in simplified and natural bulk compositions. *J. Petrol.* **40**, 629–652.

Kushiro I. (1976) A new furnace assembly with a small temperature gradient in solid-media, high-pressure apparatus. *Carnegie Inst. Wash. Year Book* **75**, 832–833.

Liu J. G., Bohlen S. R., and Ernst W. G. (1996) Stability of hydrous phases in subducting oceanic crust. *Earth Planet. Sci. Lett.* **143**, 161–171.

Mao H. K., Bell P. M., and England J. L. (1971) Tensional errors and drift of the thermocouple electromotive force in the single stage, Piston-cylinder apparatus. *Carnegie Inst. Wash. Year Book* **70**, 281–287.

Marshall W. L. and Frantz J. D. (1987) Electrical conductance measurements of dilute aqueous electrolytes at temperatures to 800°C and pressures to 4000 bars: Techniques and interpretations. In *Hydrothermal Experimental Techniques* (eds. G. C. Ulmer and H. L. Barnes), pp. 261–292. Wiley-Interscience.

McInnes B. (1996) Fluid-peridotite interactions in mantle wedge xenoliths (abstr). *EOS Trans. Am. Geophys. Union* **77**, 282.

Mibe K., Fujii T., and Yasuda A. (2002) Composition of aqueous fluid coexisting with mantle minerals at high pressure and its bearing on the differentiation of the Earth's mantle. *Gechim. Cosmochim. Acta* **66**, 2273–2286.

Morris J. D., Leeman W. P., and Tera F. (1990) The subducted component in island arc lavas: Constraints from Be isotopes and B-Be systematics. *Nature* **344**, 31–36.

Mysen B. O. (1988) *Structure and Properties of Silicate Melts.* Elsevier.

Mysen B. O. (1995) Experimental, in-situ, high-temperature studies of properties and structure of silicate melts relevant to magmatic temperatures. *Eur. J. Mineral.* **7**, 745–766.

Mysen B. O. (1998) Interaction between aqueous fluid and silicate melt in the pressure and temperature regime of the Earth's crust and upper mantle. *N. Nb. Mineral.* **172**, 227–244.

Mysen B. O. (2002a) Solubility of alkaline earth and alkali aluminosilicate components in aqueous fluids in the Earth's upper mantle. *Geochim. Cosmochim. Acta* **66**, 2421–2438.

Mysen B. O. (2002b) Water in peralkaline aluminosilicate melts to 2 GPa and 1400°C. *Gechim. Cosmochim. Acta* **66**, 2915–2928.

Mysen B. O. and Boettcher A. L. (1975) Melting of a hydrous mantle. II. Geochemistry of crystals and liquids formed by anatexis of mantle

peridotite at high pressures and high temperatures as a function of controlled activities of water, hydrogen and carbon dioxide. *J Petrol.* **16**, 549–590.

Mysen B. O. and Armstrong L. (2002) Solubility behavior of alkali aluminosilicate components in aqueous fluids and silicate melts at high pressure and temperature. *Geochim. Cosmochim. Acta* **66**, 2287–2298.

Nakamura Y. and Kushiro I. (1974) Composition of the gas phase in Mg_2SiO_4-SiO_2-H_2O at 15 kbar. *Carnegie Inst. Wash. Year Book* **73**, 255–259.

Newton R. C. and Manning C. E. (2002) Solubility of enstatite + forsterite in H_2O in deep crust/upper mantle conditions: 4 to 15 kbar and 700 to 900°C. *Gechim. Cosmochim. Acta* **66**, 41650–4176.

Osborn E. F. and Muan A. (1960) Plate 2: The system CaO-Al_2O_3-SiO_2. In *Phase Equilibrium Diagrams of Oxide Systems.* American Ceramic Society.

Pitzer K. S. (1983) Dielectric constant of water at very high temperature and pressure. *Proc. Natl. Acad. Sci. USA* **80**, 4575–4576.

Plank T. and Langmuir C. H. (1993) Tracing trace elements from sediment input to volcanic output at subduction zones. *Nature* **362**, 739–743.

Poli S. and Schmidt M. W. (1998) The high-pressure stability of zoisite and phase relationships of zoisite-bearing assemblages. *Contrib. Mineral. Petrol.* **130**, 162–175.

Riter J. C. A. and Smith D. (1996) Xenolith constraints on the thermal history of the of the mantle beneath the Colorado Plateau. *Geology* **24**, 267–279.

Rollinson H. R. and Windley B. F. (1980) Selective elemental depletion during metamorphism of Achaean granulites, Scourie, NW Scotland. *Contrib. Min. Petrol.* **72**, 257–263.

Schneider M. E. and Eggler D. H. (1986) Fluids in equilibrium with peridotite minerals: Implications for mantle metasomatism. *Geochim. Cosmochim. Acta* **50**, 711–724.

Schreyer W. (1995) Ultradeep metamorphic rocks: The retrospective viewpoint. *J. Geophys. Res.* **100**, 8353–8366.

Stalder R., Ulmer P., Thompson A. B., and Gunther D. (2000) Experimental approach to constrain second critical endpoints in fluid/silicate systems: Near-solidus fluids and melts in the system abite-H_2O. *Am. Mineral.* **85**, 68–77.

Stalder R., Ulmer P., Thompson A. B., and Gunther D. (2001) High pressure fluids in the system MgO-SiO_2-H_2O under upper mantle conditions. *Contrib. Mineral. Petrol.* **140**, 607–618.

Sudo A. and Tatsumi Y. (1990) Phlogopite and K-amphibole in the upper mantle: Implications for magma genesis in subduction zones. *Geophys. Res. Lett.* **17**, 29–32.

Swanson S. E., Kay S. M., Brearley M., and Scarfe C. M. (1987) Arc and back-arc xenoliths in Kurile-Kamchatka and western Alaska. In *Mantle Xenoliths* (ed. P. H. Nixon), pp. 303–318. Wiley.

Turner S. and Foden J. (2001) U, Th, and Ra disequilibria, Sr, Nd, and. Pb isotope and trace element variations in Sunda arc lavas: Predominance of subducted sediment component. *Contrib. Mineral. Petrol.* **142**, 43–57.

Whitehouse M. J. (1989) Pb-isotopic evidence for U-Th-Pb behaviour in a prograde amphibolite to granulite facies transition from the Lewisian Complex of north-west Scotland; implications for Pb-Pb dating. *Geochim. Cosmochim. Acta* **53**, 717–724.

Zhang Y.-G. and Frantz J. D. (2000) Enstatite-forsterite-water equilibria at elevated temperatures and pressures. *Am. Mineral.* **85**, 918–925.

Zotov N. and Keppler H. (2000) In-situ Raman spectra of dissolved silica species in aqueous fluid to 900°C and 14 kbar. *Am. Mineral.* **85**, 600–603.

Zotov N. and Keppler H. (2002) Silica speciation in aqueous fluids at high pressures and high temperatures. *Chem. Geol.* **184**, 71–82.